Two-species hard-core bosons on the triangular lattice: A quantum Monte Carlo study

Jian-Ping Lv,[1,2,*] Qing-Hu Chen,[2,3,†] and Youjin Deng[4,‡]

[1]*Department of Physics, China University of Mining and Technology, Xuzhou 221116, People's Republic of China*

[2]*Department of Physics, Zhejiang University, Hangzhou 310027, People's Republic of China*

[3]*Center for Statistical and Theoretical Condensed Matter Physics, Zhejiang Normal University, Jinhua 321004, People's Republic of China*

[4]*Hefei National Laboratory for Physical Sciences at Microscale and Department of Modern Physics, University of Science and Technology of China, Hefei 230027, People's Republic of China*

(Received 3 November 2013; published 30 January 2014)

Using worm-type quantum Monte Carlo simulations, we investigate bosonic mixtures on a triangular lattice of two species of bosons, which interact via nearest-neighbor intraspecies (V) and on-site interspecies (U) repulsions. For the case of symmetric hopping amplitude ($t_A/V = t_B/V$) and $U/V = 1$, we determine a rich ground-state phase diagram that contains double-solid, double-superfluid, supersolid (SS), solid-superfluid (solid-SF), and counterflow supersolid (CSS) states. The SS, solid-SF, and CSS states exhibit spontaneous symmetry breaking among the three sublattices of the triangular lattice and between the two species, which leads to a nonzero crystalline density wave order in each species. We, furthermore, show that the CSS and the SS states are present for $t_A/V \neq t_B/V$, and the latter even survives up to the $t_A/V \to \infty$ or $t_B/V \to \infty$ limit. The effects induced by the variation of U/V and by the imbalance of particle numbers of the two species are also explored.

DOI: 10.1103/PhysRevA.89.013628 PACS number(s): 67.85.Hj, 67.85.Fg, 75.10.Jm

I. INTRODUCTION

Ultracold bosons held in optical lattices provide an ideal realization of the single-species Bose-Hubbard model [1], and attract extensive interest from both experimental and theoretical research communities (for review, see, e.g., Refs. [2] and [3]). Recently, more and more attention has been paid to two-species bosons, where novel quantum phases can emerge due to interspecies and intraspecies interactions [4–20], which can be tuned experimentally by Feshbach resonances [21,22].

Quantum phases and phase transitions in two-species bosons on bipartite lattices with on-site interspecies interaction (U) have been extensively studied. Kuklov and Svistunov demonstrated a novel quantum phase—the so-called counterflow superfluid (CSF)—and constructed an effective Hamiltonian [5]. The CSF state features a nonzero CSF density but a vanishing pair superfluid (PSF) density between the two species. Altman *et al*. investigated the hard-core case with each species at half-integer filling ($\rho_A = \rho_B = 1/2$) within a mean-field approach and established for $U > 0$ a phase diagram on the t_A/U-t_B/U plane [6]. The phase diagram contains CSF, checkerboard solid, and superfluid (SF) phases. Using a worm-type quantum Monte Carlo method, Söyler *et al*. [7] found that in the strongly asymmetric region, the phase diagram for the square lattice differs from the mean-field result [6]. More direct evidence for the emergence of the CSF phase can come from measurement of pair-correlation functions [8]. The robustness of these quantum ordered phases against thermodynamic fluctuations was then explored by Capogrosso-Sansone *et al*. [9], and finite-temperature phase transitions were obtained for the square and simple-cubic lattices. For systems away from the half-integer fillings [10] or with attractive on-site interspecies interaction $U < 0$ [11], other quantum phases can be found, e.g., the emergence of a PSF phase in the latter. Systems of two-species soft-core bosons have also been studied [12,13].

In the past few years, significant experimental progress has been achieved and ultracold atoms can be loaded into different optical lattices, such as the triangular [23], kagomé [24], and dice [25] lattices, on which rich physics can occur due to the distinct band structure or geometric frustration, etc. [26,27]. For two-species soft-core bosons on a triangular lattice with on-site intraspecies and on-site interspecies interactions, a phase diagram has been established recently [14].

In this work, we perform extensive Monte Carlo simulations on bosonic mixtures on a triangular lattice, which are made up of two species of hard-core bosons with both on-site interspecies and nearest-neighbor intraspecies repulsions. This model was recently studied by Trousselet *et al*. using a mean-field approach combined with exact diagonalizations [15]. The organization of the paper is as follows. Section II introduces the model and presents an analysis for some limiting cases. Measured quantities are defined in Sec. III. Section IV describes numerical results, and a brief discussion is given in Sec. V.

II. MODEL

Let the two species of hard-core bosons be specified by A and B and the associated creation (annihilation) operators be $a_i^\dagger$ (a_i) and $b_i^\dagger$ (b_i); the Hamiltonian studied in this work can be written as

$$H = -t_A \sum_{\langle ij \rangle} a_i^\dagger a_j - t_B \sum_{\langle ij \rangle} b_i^\dagger b_j + V \sum_{\langle ij \rangle} \left(n_i^A n_j^A + n_i^B n_j^B \right) + U \sum_i n_i^A n_i^B - \mu \sum_i \left(n_i^A + n_i^B \right), \quad (1)$$

*phys.lv@gmail.com
†qhchen@zju.edu.cn
‡yjdeng@ustc.edu.cn

where t_A and t_B are the hopping amplitudes, and V and U are the nearest-neighbor intraspecies and on-site interspecies repulsions, respectively. The symbols $n_i^A = a_i^\dagger a_i$ and $n_i^B = b_i^\dagger b_i$ are the particle-number operators. Due to the hard-core constraint, one has $\{a_i,a_i\} = \{a_i^\dagger,a_i^\dagger\} = \{b_i,b_i\} = \{b_i^\dagger,b_i^\dagger\} = 0$ and $\{a_i,a_i^\dagger\} = \{b_i,b_i^\dagger\} = 1$. The Hamiltonian is the same as that studied in Ref. [15] and similar to that in Ref. [13].

A. Particle-hole symmetry

Employing the particle-hole transformations, $U_A^+ a U_A = a^+$ and $U_B^+ b U_B = b^+$, we have

$$U_A^+ U_B^+ H(\mu) U_B U_A = H(6V + U - \mu). \tag{2}$$

Therefore, model (1) exhibits an exact particle-hole symmetry at $\mu = 3V + U/2$. It follows that, to simulate the model with a half-integer filling factor for each species, one can perform grand-canonical simulations with $\mu = 3V + U/2$. This treatment was elaborated in Ref. [17] and also employed in a dynamical mean-field study of bosonic mixtures [16].

B. Classical limit ($t_A/V = t_B/V = 0$)

In the zero-hopping limit $t_A/V = t_B/V = 0$, Hamiltonian (1) reduces to

$$H = V \sum_{\langle ij\rangle} \left(n_i^A n_j^A + n_i^B n_j^B\right) + U \sum_i n_i^A n_i^B - \mu \sum_i \left(n_i^A + n_i^B\right). \tag{3}$$

At zero temperature, $T = 0$, thermal fluctuations are frozen, and there are two possible solid states:

(1) the 2-solid–1/3 state— two sublattices are fully occupied by A and B bosons, respectively, and the remaining one is empty; and

(2) the 2-solid–2/3 state—one sublattice is fully occupied by both A and B bosons, and the other two are fully occupied by A and B bosons, respectively.

These two solid states are both of degenerate degree 6, and the internal energies are given by

$$E_{1/3} = -2N\mu/3 \tag{4}$$

and

$$E_{2/3} = N(2V + U/3 - 4\mu/3), \tag{5}$$

where N is the number of lattice sites. The two solid states coexist at $\mu = 3V + U/2$, where $E_{1/3} = E_{2/3}$.

C. Decoupled case ($U = 0$)

For $U = 0$, the two species are decoupled and Hamiltonian (1) reduces to

$$H = \sum_{\alpha\in\{A,B\}} H_\alpha, \tag{6}$$

with

$$H_\alpha = -t_\alpha \sum_{\langle ij\rangle} \alpha_i^\dagger a_j + V \sum_{\langle ij\rangle} n_i^\alpha n_j^\alpha - \mu \sum_i n_i^\alpha. \tag{7}$$

Hamiltonian (7) describes a single species of hard-core bosons with nearest-neighbor repulsion V. It has been extensively studied by different groups [26], and a supersolid (SS) state was found in the region near the half-integer filling ($\mu = 3V$).

III. MEASURED QUANTITIES

We use the worm-type quantum Monte Carlo method to simulate Hamiltonian (1). The worm algorithm is an unbiased algorithm that works in continuous imaginary time [28]; see Refs. [29] and [30] for a review. In the simulation, the linear lattice size L took several values in the range of $12 \le L \le 72$. The inverse temperatures were mostly chosen as $\beta \equiv 1/T = L$, while simulations at lower temperatures were also performed for some cases.

To explore quantum ordered phases, we measure physical quantities such as the following:

(1) Particle density for each species $\rho_\alpha = \langle N_\alpha/N\rangle$, with N_α the particle number of species α ($\alpha \in \{A,B\}$).

(2) SF density $\rho_\alpha^S = L^{2-d}\langle W_\alpha^2\rangle/\beta$, where W is the winding number [31].

(3) Static structure factor $S_\alpha^{\mathbf{Q}} = \langle \rho_\alpha^{\mathbf{Q}} \rho_\alpha^{\dagger\mathbf{Q}}\rangle$, where $\rho_\alpha^{\mathbf{Q}} = (1/N)\sum_i n_i^\alpha \exp(i\mathbf{Q}\mathbf{r}_i)$ and $\mathbf{Q} = (4\pi/3,0)$, corresponding to $\sqrt{3}\times\sqrt{3}$ ordering.

(4) CSF stiffness $\rho_{\rm CSF} = L^{2-d}\langle (W_A - W_B)^2\rangle/\beta$, and PSF stiffness $\rho_{\rm PSF} = L^{2-d}\langle (W_A + W_B)^2\rangle/\beta$.

IV. RESULTS

Our main findings are the phase diagrams shown in Figs. 1 and 2. Figure 1 illustrates the phase diagram for $t_A/V = t_B/V$ (say, t/V) and $U/V = 1$ on the t/V-μ/V plane, which includes 2-solid–1/3, 2-solid–2/3, double-SF (2SF), SS, solid-SF, and counterflow supersolid (CSS) states. For a given t/V, the lattice is empty below chemical potential $\mu = -6t$, which is the energy to add into the lattice a pair of bosons of different species. From the particle-hole transformation, it is known that the phase boundaries are symmetric with respect to the line $\mu = 7V/2$.

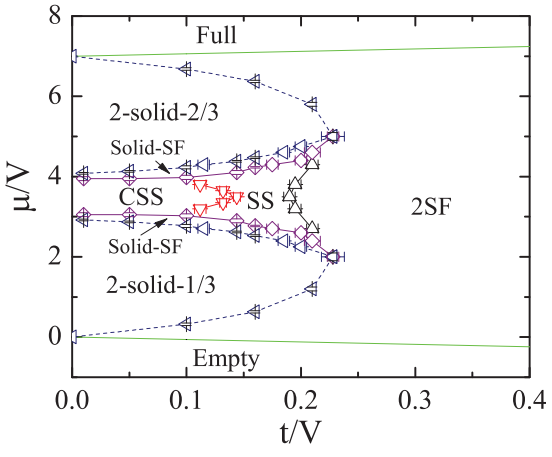

FIG. 1. (Color online) Phase diagram for $U/V = 1$ and $t_A/V = t_B/V :\equiv t/V$. Symbols represent critical points obtained from the simulations; solid and dashed lines denote continuous and discontinuous phase transitions, respectively.

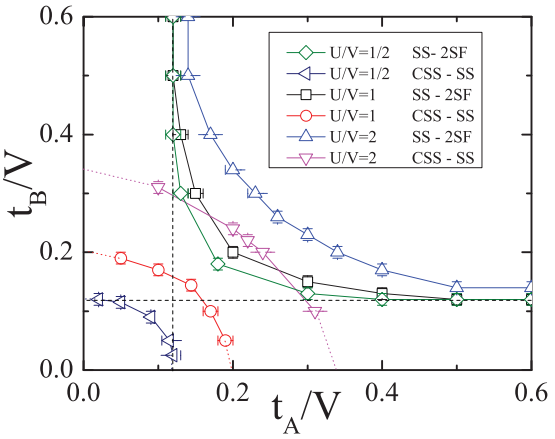

FIG. 2. (Color online) Phase boundaries for different U values at the half-integer filling of each species. Symbols represent critical points obtained from the simulations; solid lines denote phase boundaries. Dashed black lines correspond to the SS-SF transitions in model (7).

Figure 2 shows the phase boundaries on the t_A/V-t_B/V plane with each species at half-filling, for $U/V = 1/2$, 1, and 2, including the CSS, SS, and 2SF states. The quantum ordered phases can be determined by examining the robustness of measured quantities in the limit of $L \to \infty$ and $\beta \to \infty$.

(1) 2-solid–1/3 state: $\forall\ \alpha \in \{A,B\}$, $\rho_\alpha = 1/3$, $\rho_\alpha^S = 0$, $S_\alpha^{\mathbf{Q}} > 0$; $\rho_{\mathrm{CSF}} = 0$, $\rho_{\mathrm{PSF}} = 0$.

(2) 2-solid–2/3 state: $\forall\ \alpha \in \{A,B\}$, $\rho_\alpha = 2/3$, $\rho_\alpha^S = 0$, $S_\alpha^{\mathbf{Q}} > 0$; $\rho_{\mathrm{CSF}} = 0$, $\rho_{\mathrm{PSF}} = 0$.

(3) 2SF state: $\forall\ \alpha \in \{A,B\}$, $\rho_\alpha^S > 0$, $S_\alpha^{\mathbf{Q}} = 0$; $\rho_{\mathrm{CSF}} > 0$, $\rho_{\mathrm{PSF}} > 0$.

(4) CSS state: $\forall\ \alpha \in \{A,B\}$, $\rho_\alpha^S > 0$, $S_\alpha^{\mathbf{Q}} > 0$; $\rho_{\mathrm{CSF}} > 0$, $\rho_{\mathrm{PSF}} = 0$.

(5) SS state: $\forall\ \alpha \in \{A,B\}$, $\rho_\alpha^S > 0$, $S_\alpha^{\mathbf{Q}} > 0$; $\rho_{\mathrm{CSF}} > 0$, $\rho_{\mathrm{PSF}} > 0$.

(6) Solid-SF state: $\rho_A^S = 0$, $\rho_B^S > 0$ or $\rho_A^S > 0$, $\rho_B^S = 0$; $\forall\ \alpha \in \{A,B\}$, $S_\alpha^{\mathbf{Q}} > 0$; $\rho_{\mathrm{CSF}} > 0$, $\rho_{\mathrm{PSF}} > 0$.

To further explore these quantum phases, we also took snapshots of world-line configurations and performed histogram analyses.

In comparison with the classical limit, which only exhibits the 2-solid–1/3 and 2-solid–2/3 states, quantum fluctuations lead to many unusual states that break a variety of symmetries. In the 2SF state, an off-diagonal SF order develops for each species, and the U(1) × U(1) symmetry is broken. The solid-SF, SS, and CSS states exhibit simultaneously broken translational and U(1) symmetries, as well as broken symmetry between the two species.

The following subsections present numerical evidence for the aforementioned findings. Section IIA constructs the phase diagram in Fig. 1 for $t_A/V = t_B/V$ and $U/V = 1$. Section IIB determines the phase boundaries in Fig. 2 at half-integer fillings and reveals the effects induced by the variation of U/V.

A. $t_A/V = t_B/V$ and $U/V = 1$

1. Half-integer fillings

We perform grand-canonical simulations with $\mu/V = 7/2$, which yield particle density $\rho_A = \rho_B = 0.5000(1)$ [see Fig. 3(a)]. As the hopping amplitude t increases, the PSF stiffness ρ_{PSF} starts to become nonzero near $t/V \sim 0.15$, as shown in Fig. 3(b). To more precisely locate the phase transition point, we perform a finite-size scaling analysis of the ρ_{PSF} data. At the transition point, it is expected that the PSF stiffness scales as $\rho_{\mathrm{PSF}} = L^{2-d-z} f(\beta/L^z)$, where the dynamical critical exponent z equals 1 if the system has particle-hole symmetry. The inset in Fig. 3(b) plots the scaled PSF stiffness $L\rho_{\mathrm{PSF}}$ versus t/V, which yields the transition point as $t/V = 0.144(2)$ from the approximate common intersection for different L values. The $S_A^{\mathbf{Q}}$ data in Fig. 3(c) suggest another transition point at $t/V = 0.20(1)$ beyond which the crystalline order vanishes. These two transition points should separate three phases, which are identified below.

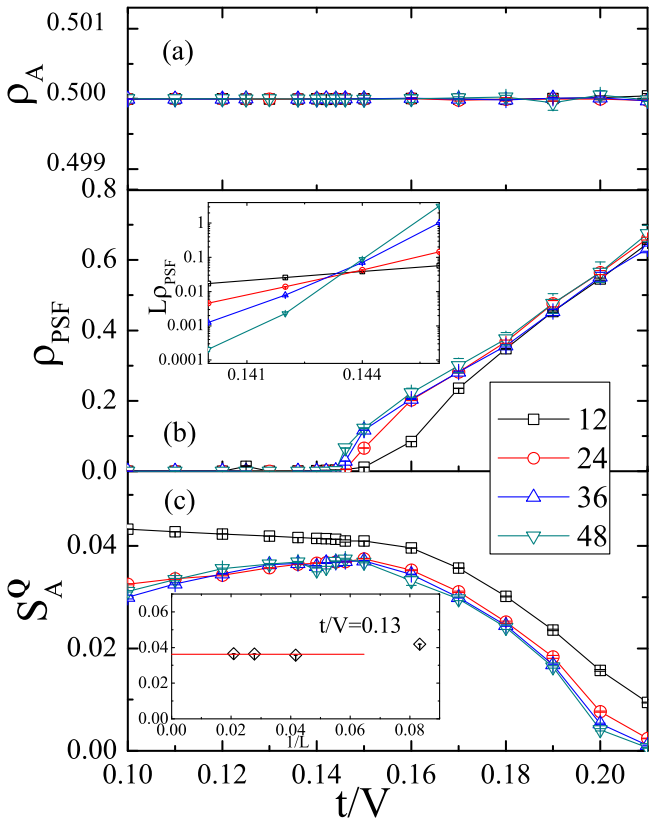

FIG. 3. (Color online) Quantities ρ_A (a), ρ_{PSF} (b), and $S_A^{\mathbf{Q}}$ (c) versus t/V at $\mu/V = 3.5$ and $U/V = 1$.

We first present numerical evidence for the CSS state in the region $t/V < 0.144(2)$. The nonzero crystalline order for each species is demonstrated in Fig. 3(c) and in the inset, which plots $S_A^{\mathbf{Q}}$ versus $1/L$ for $t/V = 0.13$. It is known [9] that the CSF density ρ_{CSF} is fragile against thermal fluctuations. Thus, to detect the CSS order, we simulate at temperature $\beta = 5L$ for $t/V = 0.13$. As shown in Fig. 4 and the inset, the CSF density ρ_{CSF} clearly approaches a nonzero value as L increases; in contrast, the PSF density ρ_{PSF} drops drastically, to 0. This evidence establishes the CSS state for $t/V < 0.144(2)$. A histogram analysis is performed to further explore the particle-number distribution. In addition to the broken U(1) symmetry due to the long-range off-diagonal order ρ_{CSF}, it is observed that both the symmetry among the three sublattices

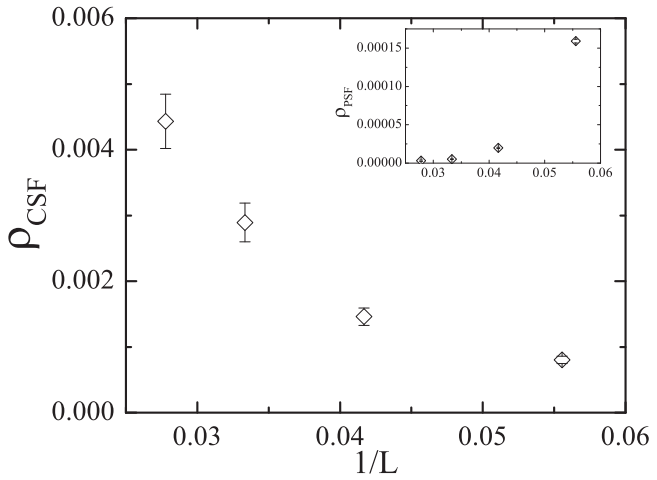

FIG. 4. Quantity ρ_{CSF} versus $1/L$ at $\mu/V = 3.5$, $t/V = 0.13$, and $U/V = 1$. Inset: ρ_{PSF} versus $1/L$. For these two figures, simulations were performed with $\beta = 5L$ (see text).

and the symmetry between the two species are spontaneously broken. Namely, the particle density $\rho_{\alpha,s}$ on sublattice s for species α can vary for different species and for different sublattices (say S_1, S_2, S_3). There are sixfold ground states, in one of which the filling factor is arranged as $(1,\frac{1}{4},\frac{1}{4})$ for A bosons and $(0,\frac{3}{4},\frac{3}{4})$ for B bosons. The bosons on sublattice S_1 are pinned, and the counter-flow superfluidity arises from S_2 and S_3, which form a honeycomb lattice. Finally, we note that despite the symmetry breaking between A and B bosons, the total particle numbers are identical for the A and B bosons; i.e., $\sum_s \rho_{\alpha,s} = 3/2$, and the summed filling factor of the two species is unity for each sublattice, i.e., $\sum_\alpha \rho_{\alpha,s} = 1$.

In the region $0.144(2) < t/V < 0.20(1)$, the system is in the SS state and characterized by a nonzero crystalline order and nonzero SF density for both species, as demonstrated in Figs. 3(b) and 3(c). In comparison with the CSS state, the degenerate degree of the ground state is also 6 but the particle distribution is distinct, arranged as $(\frac{1}{6},\frac{2}{3},\frac{2}{3})$ for one species and $(\frac{5}{6},\frac{1}{3},\frac{1}{3})$ for the other. Also, note that the two species have equal total numbers of bosons and the summed filling factor on each sublattice is unity. The bosons on the sublattice of filling factor $\left(\frac{1}{6}+\frac{5}{6}\right)$ are pinned, while those on the remaining two sublattices account for the superfluidity. Figure 5 illustrates a

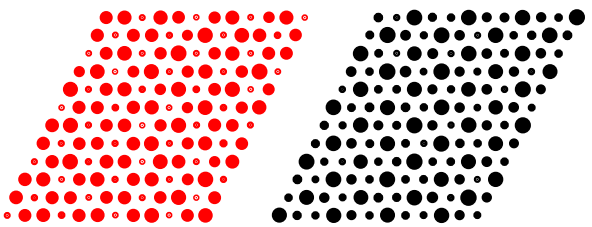

FIG. 5. (Color online) Typical particle distributions on a world-line configuration in the SS state ($t/V = 0.175$, $\mu/V = 3.5$, and $U/V = 1$) for A (left) and B (right) species, respectively. This world-line configuration was obtained after sufficient Monte Carlo steps to achieve equilibrium. The simulation was on a 36×36 lattice, but for illustrative purposes, we show a block of 12×12 sites.

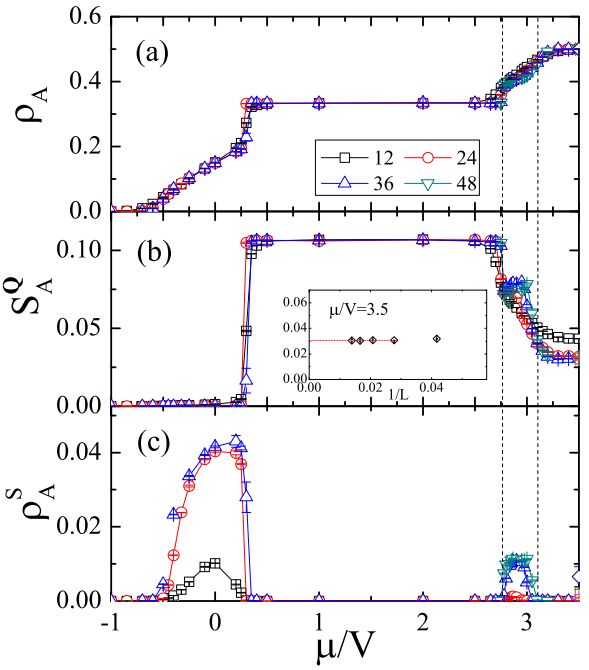

FIG. 6. (Color online) The quantities ρ_A (a), $S^{\mathbf{Q}}_A$ (b), and ρ^S_A (c) versus μ/V for $t/V = 0.1$ and $U/V = 1$. The region between the two dashed lines corresponds to the solid-SF state, for which the data are average results of Monte Carlo simulations with different initial conditions.

snapshot of the particle-number distribution for $t/V = 0.175$ and $L = 36$, which is averaged over the imaginary-time axis of a world-line configuration.

For $t/V > 0.20(1)$, the system is in a 2SF state, featuring a nonzero SF density and zero crystalline order for both species.

2. $t/V = 0.1$

We describe the simulations for $U/V = 1$ and away from the symmetric line $\mu/V = 7/2$ in the example of $t/V = 0.1$ with varying μ/V values. As the chemical potential μ increases, the system in the 2SF phase is driven into the 2-solid–1/3 state by a first-order phase transition at $\mu/V = 0.32(3)$, reflected by the discontinuities of ρ_A, ρ^S_A, and $S^{\mathbf{Q}}_A$ in Fig. 6.

In the region $2.77(2) < \mu/V < 3.10(5)$, the system is detected to be in a novel quantum state which exhibits a nonzero crystalline order for both species but a nonzero SF density for one species only. The ground state is still sixfold, and the particle distribution on sublattice (S_1,S_2,S_3) is arranged as (1,0,0) for one species—say A bosons—and $(0,\frac{3\rho_B}{2},\frac{3\rho_B}{2})$ for B bosons, where ρ_B is a function of μ/V. The A bosons are pinned on sublattice S_1 and do not exhibit a visible SF density. The B bosons are only present on sublattices S_2 and S_3 and contribute to the nonzero SF density. Unlike in the CSS and SS states, the total particle numbers of the A and B bosons are no longer identical; one has $\rho_A = (1/3)\sum_s \rho_{s,A} = 1/3$, while $\rho_B = (1/3)\sum_s \rho_{s,B}$ varies with μ/V. We provide further analyses by simulating, at a rather low temperature, $\beta = 720$ for $(\mu/V = 2.9, L = 36)$. We define a vector order parameter for each species $\vec{n}_\alpha = \rho_{1,\alpha} + \rho_{2,\alpha}e^{i2\pi/3} + \rho_{3,\alpha}e^{i4\pi/3}$ ($\alpha = A$

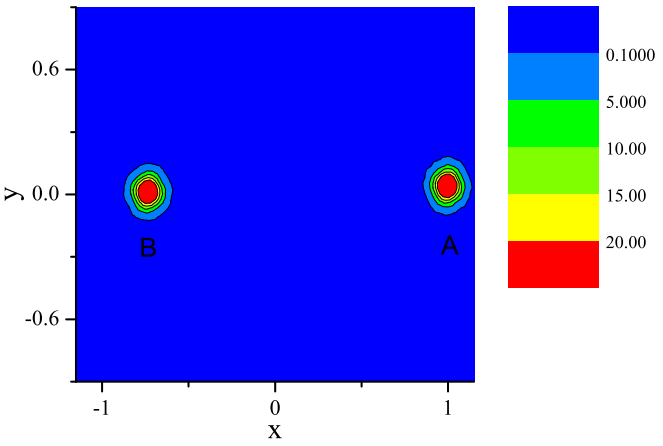

FIG. 7. (Color online) Histogram of quantities $\vec{n}_A$ and $\vec{n}_B$ obtained from a single simulation in the solid-SF state. The simulation is for the parameter set $t/V = 0.1$, $\mu/V = 2.9$, $U/V = 1$, $L = 36$, and $\beta = 720$ and determines $\rho_A = 0.333(1)$ and $\rho_B = 0.480(1)$. The determined particle density of species A is consistent with the expected value $1/3$ (with a tiny relative error), providing more evidence supporting the formation ofa commensurate solid by species A.

and B). The histogram is shown in Fig. 7, where the probability distribution of $\vec{n}_A$ is around point (1,0) and that of $\vec{n}_B$ is around point $(-\frac{3\rho_B}{2},0)$ with $\rho_B = 0.480(1)$. The imbalance of the total particle numbers of the two species is clearly seen. A snapshot of the particle distribution is shown in Fig. 8. A nonzero SF density ρ_B^S is observed, while ρ_A^S is 0.0000(1), consistent with 0. Note that the density wave of the B species is induced by the A species, which forms an insulating solid. Therefore, the B species should be known as SF rather than SS, and the mixture can be called solid-SF. This treatment was also discussed in Ref. [7]. We conclude this paragraph by mentioning the following. In Ref. [15], a similar phase was observed away from the half-filling case in the parameter region including $(U/V = 2, t/V = 0.15)$, which is characterized by a threefold order for both species and a nonzero SF density for one species only. This phase was referred to the supersolid–threefold-order (SS-3FO) phase. However, according to Ref. [15], the SS-3FO phase has a rather distinct particle distribution: two sublattices are respectively filled by the two species, while in the remaining sublattice,

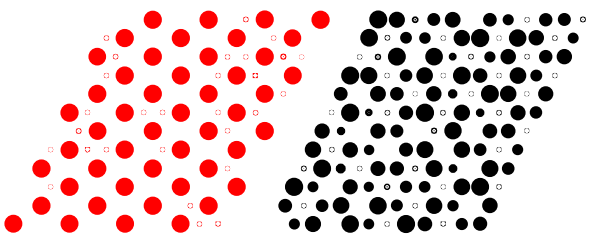

FIG. 8. (Color online) Typical particle distribution in a world-line configuration in the solid-SF state ($t/V = 0.1$, $\mu/V = 2.9$, and $U/V = 1$) for species A (left) and B (right), respectively. This world-line configuration was obtained after sufficient Monte Carlo steps to achieve equilibrium. The simulation is on a 36×36 lattice, but for illustrative purposes, we show a block of 12×12 sites.

a species of bosons accounts for the superfluidity. This is inconsistent with our observation for the solid + SF phase, in which the superfluidity arises from one species of bosons on two sublattices that form a honeycomb lattice.

For the region $3.10(5) < \mu/V \leqslant 3.5$, the system is in the CSS state, supported by the robust crystalline order for each species together with the vanishing pair superfluidity and nonzero counterflow superfluidity.

The whole phase diagram in Fig. 1 is constructed by simulations with a variety of $(t/V, \mu/V)$ values.

B. $t_A/V \neq t_B/V$ and/or $U/V \neq 1$

In this subsection, we study the effects induced by the asymmetry between the A and the B bosons due to imbalanced hopping amplitudes $t_A/V \neq t_B/V$. The effects caused by tuning interaction U/V are also considered.

1. $U/V = 1$ and $\mu/V = 7/2$

We first study the $t_A/V \neq t_B/V$ effect for $(U/V = 1, \mu/V = 7/2)$, with each species at half-integer filling. We simulate at $t_A/V = 0.05$ with varying t_B/V, and Fig. 9(a) shows $L\rho_{\rm PSF}$ for different L values, indicating a continuous phase transition at $t_B/V = 0.19(1)$. Near this point, a kink is observed in $S_A^{\rm Q}$ [Fig. 9(b)]. Nevertheless, no sharp decrease in $S_A^{\rm Q}$ exists on either side of the transition; actually, $S_A^{\rm Q}$ in the whole t_B/V range converges to nonzero values as $L \to \infty$. A finite-size analysis is shown in the inset in Fig. 9(b) for $t/V = 0.45$. A similar feature is found for $S_B^{\rm Q}$ [Fig. 9(c)]. This means that both species exhibit a crystalline order over the whole t_B/V range. Together with the behavior of $\rho_{\rm CSF}$ (not

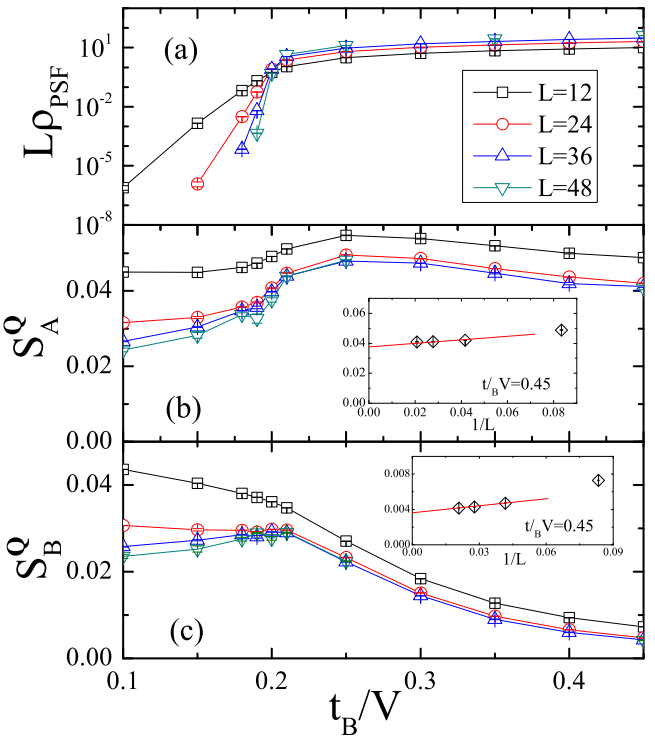

FIG. 9. (Color online) Quantities $L\rho_{\rm PSF}$ (a), $S_A^{\rm Q}$ (b), and $S_B^{\rm Q}$ (c) versus t_B/V at $t_A/V = 0.05$ and $U/V = 1$.

shown), it can be established that the system is in the CSS state for $t_B/V < 0.19(1)$ and the SS state for $t_B/V > 0.19(1)$.

It is interesting to note that as t_B/V increases, the crystalline order of B bosons is not destroyed. The underlying reason is that such an order is induced by the translational symmetry breaking due to A bosons which are in the SS state.

Simulations have been carried out for a variety of t_A/V values for ($U/V = 1$, $\mu/V = 7/2$). The phase diagram in the (t_A/V,t_B/V) plane (Fig. 2) contains the CSS, SS, and 2SF states.

2. U/V varies

To study the effects induced by variation of the interaction ratio U/V, we simulate for $U/V = 1/2$ and 2 at half-integer filling ($\mu = 3V + U/2$). The phase diagrams (Fig. 2) for different U/V values are of similar topology and contain two phase boundaries separating the CSS, SS, and 2SF states. As U/V increases, the CSS region gets broader, while the SS phase near the symmetric line $t_A/V = t_B/V$ drastically shrinks. As U/V decreases, the SS-2SF phase boundary gets closer and closer to $t_A/V \approx 0.12$ or $t_B/V \approx 0.12$, which are the SS-SF transition points of model (7) (denoted dashed black lines in Fig. 2) [26]. The SS state is persistent up to asymmetric hopping limits ($t_A/V \to \infty$, $t_B/V \lessapprox 0.12$) and ($t_A/V \lessapprox 0.12$, $t_B/V \to \infty$).

V. DISCUSSION

We have explored the quantum ordered phases in bosonic mixtures on a triangular lattice, which are constituted by two species of hard-core bosons, by using extensive Monte Carlo simulations. These quantum ordered phases are determined by complementary approaches: examining the robustness of measured quantities, analyzing world-line configurations, and performing histogram analyses. For $t_A/V = t_B/V$ (say, t/V) with $U/V = 1$, we constructed a complete ground-state phase diagram (Fig. 1) in the t/V-μ/V plane, which includes 2-solid–1/3, 2-solid–2/3, 2SF, SS, solid-SF, and CSS states. We then considered cases with $t_A/V \neq t_B/V$ and found that the SS and CSS states are present in a broad parameter range (Fig. 2). Further, the SS state even survives up to the asymmetric limits of hopping amplitudes. We also explored the effects induced by variation of the interaction ratio U/V, which is experimentally tunable.

In the CSS, SS, and solid-SF states, both the symmetry among the three sublattices and the symmetry between the two species are spontaneously broken, and the ground state is sixfold. To further check the robustness of these states and the sixfold degeneracy, we slightly break the balance of the chemical potentials of the two species such that $\mu_A = \mu + 0^+$ and $\mu_B = \mu + 0^-$. No qualitative change is observed in the CSS state, but the SS and solid-SF states both become threefold. In the SS state, A bosons prefer the filling arrangement ($\frac{1+0^+}{6}, \frac{2+0^+}{3}, \frac{2+0^+}{3}$), while the B species is of the ($\frac{5+0^-}{6}, \frac{1+0^-}{3}, \frac{1+0^-}{3}$) structure. In the solid-SF phase with $\mu < 3V + U/2$, the B species is in the solid state with filling factor (1,0,0), while the A bosons are in the SF phase. This demonstrates that the whole region of the SS and solid-SF states is a surface of first-order phase transitions.

While finishing most of the Monte Carlo simulations for this paper, we became aware of the recent work by Trousselet *et al*. [15], who studied the same system with a mean-field approach and exact diagonalizations. While most of the quantum phases in our work have already been predicted in Ref. [15], a quantitative difference does exist in the location of phase boundaries. Furthermore, via snapshots of world-line configuration and histogram analyses, this work provides strong and direct evidence for the CSS, SS, and solid-SF phases, which are, respectively, termed the "color supersolid," "bosonic pinball," and "SS-3FO" phases in Ref. [15]. Finally, the filling factors in the solid-SF phase are found to be qualitatively different.

Experimental studies of bosonic mixtures on triangular optical lattices are called for to test the novel quantum phases in this work and in Ref. [15]. Since the present model has many tunable parameters, other nontrivial quantum ordered states which are located in certain parameter ranges may be still uncovered, which request further theoretical work. For example, a pair-SS state may emerge if the on-site interspecies interaction becomes attractive ($U < 0$) [13]. The present algorithm is potentially applicable in some spin-boson models such as those in Refs. [32] and [33].

ACKNOWLEDGMENTS

This paper received great help from Nikolay Prokof'ev and Boris Svistunov, who shared code with us, made a critical reading of the manuscript, and provided insightful suggestions. This work was supported by the National Basic Research Program of China (Grants No. 2011CBA00103 and No. 2011CB921304), the National Natural Science Foundation of China (Grants No. 11147013 and No. 11275185), and Fundamental Research Funds for the Central Universities (Grants No. 2012QNA43 and No. 2011RC25).

[1] M. Greiner, O. Mandel, T. Esslinger, T. W. HaEnsch, and I. Bloch, Nature **415**, 39 (2002).
[2] M. Lewenstein, A. Sanpera, V. Ahufinger, B. Damski, A. Sen, and U. Sen, Adv. Phys. **56**, 243 (2007).
[3] O. Morsch and M. Oberthaler, Rev. Mod. Phys. **78**, 179 (2006).
[4] M. Boninsegni, Phys. Rev. Lett. **87**, 087201 (2001).
[5] A. B. Kuklov and B. V. Svistunov, Phys. Rev. Lett. **90**, 100401 (2003).
[6] E. Altman, W. Hofstetter, E. Demler, and M. D. Lukin, New J. Phys. **5**, 113 (2003).
[7] S. G. Soyler, B. Capogrosso-Sansone, N. V. Prokof'ev, and B. V. Svistunov, New J. Phys. **11**, 073036 (2009).
[8] T. Ohgoe and N. Kawashima, Phys. Rev. A **83**, 023622 (2011).
[9] B. Capogrosso-Sansone, S. G. Soyler, N. V. Prokof'ev, and B. V. Svistunov, Phys. Rev. A **81**, 053622 (2010).
[10] K. Hettiarachchilage, V. G. Rousseau, K. M. Tam, M. Jarrell, and J. Moreno, Phys. Rev. B **88**, 161101(R) (2013).

[11] P. Chen, and M. F. Yang, Phys. Rev. B **82**, 180510(R) (2010).
[12] M. Guglielmino, V. Penna, and B. Capogrosso-Sansone, Phys. Rev. A **82**, 021601(R) (2010).
[13] C. Trefzger, C. Menotti, and M. Lewenstein, Phys. Rev. Lett. **103**, 035304 (2009).
[14] L. He, Y. Li, E. Altman, and W. Hofstetter, Phys. Rev. A **86**, 043620 (2012).
[15] F. Trousselet, P. Rueda, and A. Ralko, arXiv:1304.4258v1.
[16] A. Hubener, M. Snoek, and W. Hofstetter, Phys. Rev. B **80**, 245109 (2009).
[17] K. Pakrouski, Master's thesis, ETH Zurich (2011).
[18] M. Iskin, Phys. Rev. A **82**, 033630 (2010).
[19] K. Kataoka, Y. Kuno, and I. Ichinose, J. Phys. Soc. Jpn. **81**, 124502 (2012).
[20] Y. Kuno, K. Kataoka, and I. Ichinose, Phys. Rev. B **87**, 014518 (2013).
[21] J. Catani, L. De Sarlo, G. Barontini, F. Minardi, and M. Inguscio, Phys. Rev. A **77**, 011603(R) (2008).
[22] G. Thalhammer, G. Barontini, L. De Sarlo, J. Catani, F. Minardi, and M. Inguscio, Phys. Rev. Lett. **100**, 210402 (2008).
[23] J. Struck, C. Olschlager, R. L. Targat, P. Soltan-Panahi, A. Eckardt, M. Lewenstein, P. Windpassinger, and K. Sengstock, Science **333**, 996 (2011); C. Becker, P. Soltan-Panahi, J. Kronjager, S. Dorscher, K. Bongs, and K. Sengstock, New J. Phys. **12**, 065025 (2010).
[24] G. B. Jo, J. Guzman, C. K. Thomas, P. Hosur, A. Vishwanath, and D. M. Stamper-Kurn, Phys. Rev. Lett. **108**, 045305 (2012); J. Ruostekoski, *ibid.* **103**, 080406 (2009).
[25] G. Moller and N. R. Cooper, Phys. Rev. Lett. **108**, 045306 (2012).
[26] S. Wessel and M. Troyer, Phys. Rev. Lett. **95**, 127205 (2005); D. Heidarian and K. Damle, *ibid.* **95**, 127206 (2005); R. G. Melko, A. Paramekanti, A. A. Burkov, A. Vishwanath, D. N. Sheng, and L. Balents, *ibid.* **95**, 127207 (2005); M. Boninsegni and N. Prokof'ev, *ibid.* **95**, 237204 (2005).
[27] S. V. Isakov, S. Wessel, R. G. Melko, K. Sengupta, and Y. B. Kim, Phys. Rev. Lett. **97**, 147202 (2006).
[28] N. V. Prokof'ev, B. V. Svistunov, and I. S. Tupitsyn, Sov. Phys. JETP **87**, 310 (1998).
[29] N. V. Prokof'ev and B. V. Svistunov, in *Understanding Quantum Phase Transitions*, edited by Lincoln D. Carr (Taylor & Francis, Boca Raton, 2010).
[30] L. Pollet, Rep. Prog. Phys. **75**, 094501 (2012).
[31] E. L. Pollock and D. M. Ceperley, Phys. Rev. B **36**, 8343 (1987).
[32] A. Winter, H. Rieger, M. Vojta, and R. Bulla, Phys. Rev. Lett. **102**, 030601 (2009).
[33] Y. Y. Zhang, Q. H. Chen, and K. L. Wang, Phys. Rev. B **81**, 121105(R) (2010).